

# On the CCD Calibration of Zwicky galaxy magnitudes & The Properties of Nearby Field Galaxies

E. Gaztañaga<sup>1</sup> and G. B. Dalton<sup>2</sup>

<sup>1</sup>*Consejo Superior de Investigaciones Científicas (CSIC), Institut d'Estudis Espacials de Catalunya (IEEC), Edf. Nexus-104 - c/ Gran Capitan 2-4, 08034 Barcelona, Spain.*

<sup>2</sup>*Astrophysics, University of Oxford, Keble Road, Oxford, OX1 3RH, UK.*

2 December 2024

## ABSTRACT

We present CCD photometry for galaxies around 204 bright ( $m_Z < 15.5$ ) Zwicky galaxies in the equatorial extension of the APM Galaxy Survey. We fit a best linear relation between the Zwicky  $m_Z$  system and the CCD photometry by doing a likelihood analysis that corrects for Malmquist bias. This fit yields a large scale error in Zwicky of  $\Delta m_Z \simeq (0.62 \pm 0.05) \Delta B_{CCD}$  and a mean zero point of  $\langle B_{CCD} - m_Z \rangle = -0.35 \pm 0.15$  mag. The scatter around this fit is about 0.4 mag. We find a significant positive angular correlation of both Zwicky and CCD magnitudes and positions in the sky at scales smaller than about 5 arcmin, which corresponds to  $\lesssim 100 h^{-1}$  Kpc. The Zwicky scale error is also apparent in these angular correlations. Correcting the Zwicky magnitude system with the best fit model results in a 60% lower normalization and 0.35 mag brighter  $M_*$  in the luminosity function. This brings the CfA2 luminosity function closer to the other low redshift estimations (eg Stromlo-APM or LCRS). We also present colors, sizes and ellipticities for galaxies in our fields which provides a good local reference for the studies of galaxy evolution.

**Key words:** Galaxies: Evolution ; Galaxies: Clustering ; Cosmology ; Large-scale structure of the universe

## 1 INTRODUCTION

Some important aspects of galaxy evolution can only be understood by studying the statistical properties of nearby field galaxies, in particular the luminosity function (LF). As well as providing vital information for galaxy evolution studies, an accurate knowledge of the present day LF is needed to normalize the number counts of galaxies at faint magnitudes, and to understand the clustering and large scale structure of the galaxy distribution. Moreover, the color distribution of the nearby galaxies provides a basic reference to determine star formation rates in galaxies.

Much recent work has been directed towards studying the evolution of the LF using samples of faint galaxies at high-redshift, but a consideration of the ensemble of available estimates of the LF at low redshifts suggests that there are still large inconsistencies which must be reconciled before reliable conclusions can be drawn about the implications of deep surveys.

It is common practice to fit the LF to the so called Schechter (1976) form:

$$\phi(L) = \phi_* \left(\frac{L}{L_*}\right)^\alpha \exp\left(-\frac{L}{L_*}\right), \quad (1)$$

were luminosity is related with magnitude in the usual way,  $\frac{L}{L_*} = 10^{0.4(M_* - M)}$ . Determinations of the low redshift  $B$ -band LF are available from the Stromlo-APM Survey (SAPM, Loveday et al., 1992), the Southern Sky Redshift Survey (Da Costa et al., 1994), the CfA2 redshift survey (Marzke et al., 1994), and more recently from the ESO Slice Project (Zucca et al., 1997) and the 2dF Galaxy Redshift Survey (Folkes et al., 1999). Determinations in the  $R$ -band are available from the Las Campanas Redshift Survey (LCRS, Lin et al., 1994) and from the Century Survey (CS, Geller et al., 1997). The best determinations of the Schechter function parameters from each of these surveys are listed in Table 1.

After making a zero-point adjustment to account for the difference in blue and red magnitudes, the final six rows of Table 1 are all in reasonable agreement, with only the CfA2 result showing a large deviation, particularly in the value of  $\phi_*$ . The difference in the LFs deduced from the CfA2 and SAPM surveys is illustrated in Figure 1.

At face value, the CfA2 LF seems to have less intrinsically bright galaxies (at least 10 times less  $M = -21$  galaxies). Of course, this depends on the transformation between Zwicky  $m_Z$ , APM  $b_j$  or LCRS  $R$  magnitudes. Efstathiou *et*

Survey	Band	$N_{gal}$	$\bar{z}$	$M_*$	$\alpha$	$\phi_*$ $h^3 \text{Mpc}^{-3}$
CfA2	$m_Z$	9063	0.025	-18.8	-1.0	0.040
SSRS2	$b_J$	2919	0.025	-19.5	-1.2	0.015
SAPM	$b_J$	1658	0.050	-19.5	-1.0	0.014
ESP	$b_J$	4044	0.1	-19.6	-1.2	0.020
2dF	$b_J$	5869	0.14	-19.7	-1.3	0.017
LCRS	$R$	18678	0.1	-20.3	-0.7	0.019
CS	$R$	1762	0.06	-20.7	-1.2	0.025

**Table 1.** Luminosity Function parameters derived from currently available surveys.

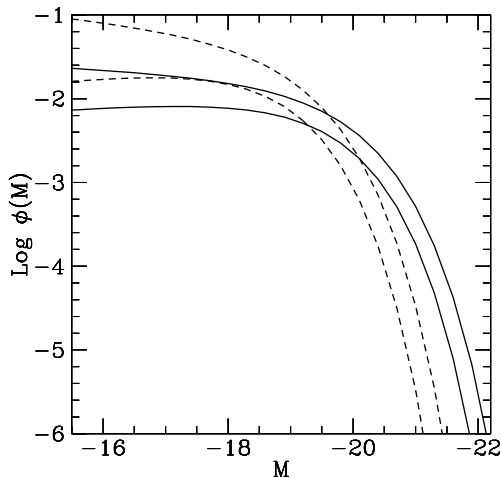


**Figure 1.** Luminosity function estimations in the SAPM and the CfA2 as a function of absolute magnitudes  $M$  in each magnitude system ( $b_J$  or  $m_Z$ ). The continuous lines enclose the 2-sigma region in the SAPM estimation whereas the dashed lines enclose the 2-sigma region in the CfA2 estimate.

*al.* (1988) adopted the relation  $m_Z = B_T + 0.29$  for the CfA1 survey. This transformation would move the CfA2 LF in the correct direction to reconcile it with other measurements, although Lin et al. (1994) point out that a shift of 0.7 mag in  $M$  is required to reconcile  $M_*$  with the other surveys. However, a simple shift in the magnitude zero-point would not correct for the apparent discrepancy in the normalisation, which would suggest that a more subtle effect is present in the CfA2 data.

In this paper we present the results of a photometric survey of bright galaxies in the overlap region of CfA2 and the equatorial extension of the APM Galaxy Survey (Maddox, 1991), which we will use to investigate this apparent discrepancy. In Section 2 we begin by comparing the APM photometry with the Zwicky measurements. We describe our CCD observations in Section 3, and compare our observations with Zwicky’s photometry in Section 4. In Section 5 we give some other properties for the galaxies in our fields. In Section 6 we compare our results with the findings of other authors and discuss the possible implications for other results. No direct CCD calibration has yet been published for this part of the APM Galaxy Survey. We will present a detailed comparison of our CCD photometry with the APM

data down to the survey completeness limit in a separate paper.

## 2 A COMPARISON OF ZWICKY AND APM MAGNITUDES

From the information used to calibrate the APM survey we would expect  $B_T \sim b_J^{\text{APM}} + 0.2$ , given the mean  $(B - V) \sim 0.7$  and the color equation  $b_J = B - 0.28(B - V)$  (Blair & Gilmore 1982; Maddox et al. 1990b; although this shift could increase by as much as 0.07 mag according to the findings of Metcalfe, Fong & Shanks, 1995). Adopting the relation between  $m_Z$  and  $B_T$  used by Efstathiou, Ellis & Peterson (1988), this transformation would imply

$$m_Z \sim b_J + 0.6, \quad (2)$$

which is close to the shift in  $M_*$  adopted by Lin et al. (1996), and, if taken as they stand, would suggest that the results of the two surveys might be consistent, at least in  $M_*$ .

We investigated the usefulness of this relation by considering the subset of  $\sim 100$  galaxies found in the part of the APM Galaxy Survey equatorial extension which overlaps with the Southernmost region of CfA2 (The S+3 sample of Marzke et al., 1994). This sample is drawn entirely from volume  $V$  of the Zwicky catalogue. We have used the publicly available CfA catalogue (Huchra et al. 1983) as our source for Zwicky galaxies, with magnitudes corrected as described in Huchra et al. (1983). Marzke et al find this sample to be representative of the whole of the Southern part of CfA2 (their Figure 3). We inspected this sample of galaxies on the film copies of the UKST IIIa-J Sky Survey plates, and examined the image maps as reconstructed from the APM survey data. We removed from our sample all those galaxies which had either been broken up into multiple image components or which were composed of multiple components which had been merged into a single object by the APM software. The distribution of these objects in the  $m_Z, b_J$  plane is shown in Figure 2. A simple least squares fit to these data with the slope constrained to be unity gives a zero-point shift of

$$m_Z = b_J - 0.6 \pm 0.5, \quad (3)$$

which is more than a magnitude in the opposite sense to that implied by Equation [2]. As will be noted below a more proper calibration needs the Malmquist bias correction.

The APM Survey is internally calibrated by matching images in plate overlaps, with the overall zero-point fixed by a number of CCD frames distributed over the survey region (Maddox et al., 1990b). At bright magnitudes ( $b_J \lesssim 17$ ) the calibrations are less well determined due to a combination of variations in galaxy surface brightness profiles and the smaller number of bright galaxies found in the plate overlap regions. The equatorial survey extension has been calibrated by matching to the original survey using plate overlaps and the adopted zero-point for the whole survey taken from the original CCD photometry. Maddox et al. (1990b) also used their CCD frames to perform an internal consistency check on the quality of the plate-plate matching technique, and found the residual zero point errors on individual plates to be  $\lesssim 0.04$  mag. The individual uncertainties in galaxy magnitudes in the APM system are therefore expected to be much smaller than effect shown in Figure 2. It is possible

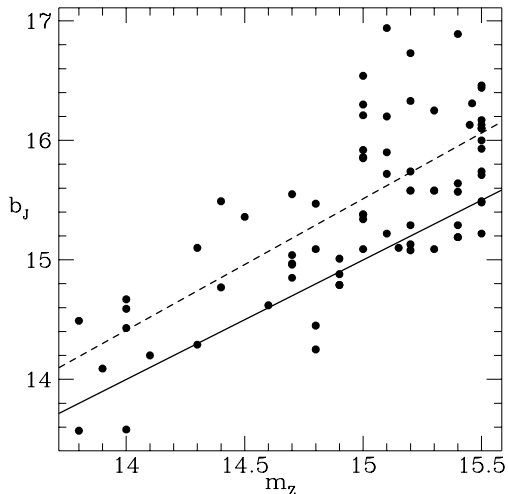


**Figure 2.** Comparison of the apparent magnitudes for a sample of  $\sim 100$  galaxies in the overlap region of the SAPM and the CfA2. Magnitudes in the SAPM catalogue correspond to APM  $b_J$  estimations while magnitudes in the CfA2 are Zwicky magnitudes,  $m_Z$ . The continuous line corresponds to  $b_J = m_Z$  and the dashed line is the best linear fit,  $m_Z = b_J - 0.6 \pm 0.5$ , showing both an off-set and a large scatter. We would expect to find at least  $m_Z = b_J + 0.5$

that an improvement in the quality of the plate material used for the more recent plates of the equatorial extension coupled with changes in the plate copying process could result in a small change in the saturation correction required for bright galaxies, and that this could produce an effect in this direction (Maddox, private communication). However, account was taken of such effects in the construction of the equatorial extension, and any residual effect is likely to be much smaller than the discrepancy shown here.

The transformation of Zwicky magnitudes to  $B_T$  deduced by Efstathiou, Ellis & Peterson (1988) are based on a comparison of the CfA1 survey data with the Durham–AAT redshift survey using 139 galaxies (Peterson et al. 1986). These authors find that the different volumes of the Zwicky catalogue have large variations in the zero-points, although volume V is found to be representative of the calibration as estimated from all volumes. These data are limited to  $m_Z < 14.5$ , and the luminosity function parameters inferred for the CfA1 are consistent with the parameters listed for the other surveys in Table 1. It is not possible to draw a direct comparison of the APM data with Zwicky data brighter than  $m_Z \sim 14$ , due to heavy saturation of galaxies this bright in the APM data. The most plausible inference from the comparison described above would therefore be a difference in the magnitude *scales* of the two surveys for  $b_J \gtrsim 14$ , with the calibration of Efstathiou, Ellis & Peterson (1988) being appropriate for the Zwicky system at brighter magnitudes.

### 3 CCD DATA

#### 3.1 CCD Observations

We used the galaxies from the sample discussed in the previous section as the basis for a CCD survey to investigate the

above discrepancy by providing an independent calibration for both surveys. This overlap region is essentially defined as  $21^{\text{h}}50 < \alpha < 3^{\text{h}}40$  and  $-0.25^\circ < \delta < 0.25^\circ$ . We obtained images with the 2.5m Isaac Newton Telescope (INT) and 1.0m Jacobus Kapteyn Telescope (JKT) in October 1994. The decision to use two telescopes was motivated by the number of close groups of Zwicky galaxies in the region, so that we use the  $10'$  field of view available at the INT to image cluster fields containing groups of bright galaxies and the  $6'$  field of view of the JKT to image individual galaxies. We used identical Tektronix  $1024 \times 1024$  detectors (TEK3 and TEK4) and Harris  $B$  filters on the two telescopes. We obtained observations of 58 fields in two nights at the INT and 73 fields in three nights at the JKT with exposure times of 360s and 600s, respectively. We observed a number of photometric standards from the list of Landolt (1992), at hourly intervals throughout each night, as well as the field of the Active Galaxy AKN120 which contains a number of photometric standards (Hamuy & Maza, 1989).

The data were reduced using standard techniques as implemented in the IRAF `ccdred` packages, with the exception that we used a modified version of the overscan correction routine to compensate for a saturation of the preamplifier used with TEK4 on the JKT. This effect manifested itself as a sudden drop in the overscan level following readout of particularly bright stellar objects in the field, and subsequent exponential recovery to the normal level as the next  $\sim 100$  rows were read out. We found that this problem could be corrected by fitting the overscan regions on either side of the drop for those fields where the effect occurred.

Extinction coefficients were derived each night, giving values in the range  $0.10 \leq k_B \leq 0.12$ . We determined zero-points for the two combinations of telescope and detector to be

$$B_{0,INT} = 24.16 \pm 0.02, \quad (4)$$

and

$$B_{0,JKT} = 21.77 \pm 0.02. \quad (5)$$

We also obtained  $R$ -band images of our standards and target fields, with zero points determined to be  $R_{0,INT} = 24.33 \pm 0.1$  and  $R_{0,JKT} = 22.11 \pm 0.02$ , but we were unable to determine any significant color term from our standard stars, consistent with previous experience with this combination of CCD and filters which are designed to be very close to the Johnson–Cousins system.

#### 3.2 Image Detection and Photometry

We used the STARLINK PISA image detection and photometry software for our photometric analysis. This is essentially the same as the image detection software used in the construction of the APM Galaxy Survey (Irwin, 1986). The basic input parameters for the detection are the threshold intensity per pixel or surface brightness,  $I_s$ , and the minimum size of the object to be detected,  $A_s$ . Amongst other parameters PISA returns total area  $A_T$ , the ellipticities and the isophotal magnitude  $B_I$  or the corresponding total magnitude  $B_T$  resulting from a curve of growth analysis for each detected object after removal of any overlapping objects.

Given that our CCD survey was designed to provide a calibration of both the APM and Zwicky data, we were

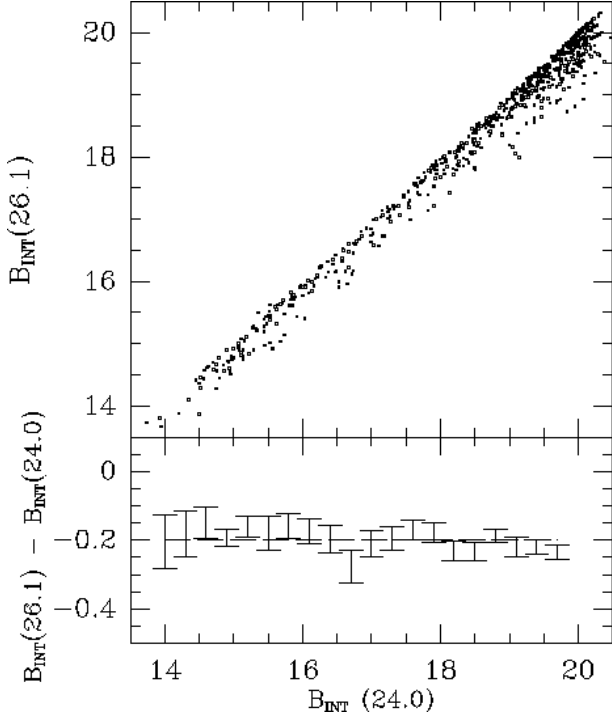


**Figure 3.** Comparison of total magnitudes  $B_{INT}$  for different isophotes:  $I = 26.1$  mag arcsec $^{-2}$  to  $I = 24.0$  mag arcsec $^{-2}$ .

	$I_s$ mag arcsec $^{-2}$	$A_s$ arcsec $^2$
INT1	26.1	96
INT2	25.7	34
INT3	25.4	34
INT4	25.0	17
INT5	24.6	10
INT6	24.4	10
<hr/>		
JKT1	25.0	12
JKT2	24.5	12
JKT3	24.1	6
JKT4	23.7	6
JKT5	22.9	3

**Table 2.** Input parameter sets used for image analysis.

necessarily interested in a wide range of magnitudes ( $14 \leq B \leq 20$ ) and image sizes. For this range of objects there was no unique combination of  $I_s$  and  $A_s$  that could deblend the faint objects without breaking the bright ones. In order to automate this process as much as possible for the whole range of magnitudes, we ran PISA several times with different combinations of  $I_s/A_s$ . These are listed in Table 2.

We chose a larger (smaller) area for the fainter (brighter) isophotes so as to select similar objects in all runs. Objects in the final catalogue were selected from the INT4 and JKT4 runs. The information from different isophotes was then used to perform an automatic rejection of broken or contaminated images. After rejection, the total magnitude and size were the largest remaining estimates of  $B_T$  and  $A_T$ , which typically correspond to the faintest isophote left. The error in  $B_T$  was taken to be the variance in the different esti-

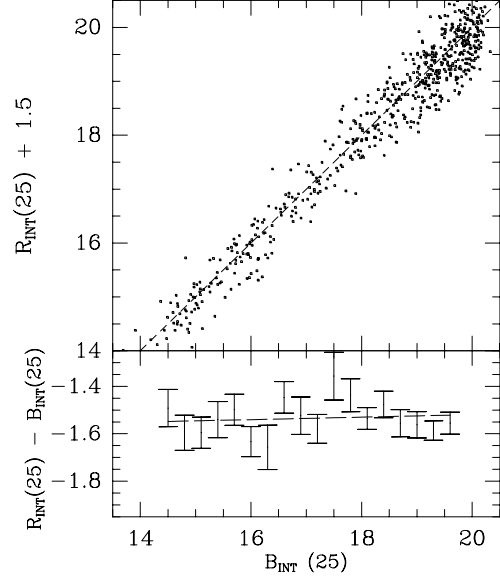


**Figure 4.** The top panel shows the red magnitudes  $R_{CCD}$  for the INT galaxies as a function of the blue  $B_{CCD}$  ones. The bottom panel shows the color  $R_{CCD}-B_{CCD}$  evolution as a function  $B_{CCD}$ .

mates for total magnitudes. Objects with rejected isophotes were automatically labeled and checked visually. We refer to total magnitudes estimated in this way as  $B_{INT}$  and  $B_{JKT}$  for the INT and JKT sets, respectively, or  $B_{CCD}$  in general. These effectively correspond to total magnitudes detected at isophotes 26.1 mag arcsec $^{-2}$  and 25.0 mag arcsec $^{-2}$ , respectively, unless stated otherwise.

To check if our isophotes are low enough we have also compute total magnitudes determined by PISA at higher isophotes. We find a small zero-point shift of the  $B_{INT}$  scale as a function of the isophote  $I$ , but for a given  $I$  this shift is not a function of  $B_T$  over the wide magnitude range considered here. This is illustrated in Figure 3 which shows a change of  $\approx 0.2$  mag in the mean  $B_{INT}(I)$  when we change the isophote from  $I = 26.1$  mag arcsec $^{-2}$  to  $I = 24.0$  mag arcsec $^{-2}$ . Changing the isophote from  $I = 26.1$  mag arcsec $^{-2}$  to  $I = 25$  mag arcsec $^{-2}$  introduces a change of only 0.1 mag. Changing the detection isophote from from  $I = 26.1$  mag arcsec $^{-2}$  to  $I = 24.4$  mag arcsec $^{-2}$  also introduces a change in  $B_{INT}$  of about 0.2 mag. We therefore conclude that the residuals associated with our final choice of detection isophote are small compared to the shifts illustrated in Figure 2.

This analysis also implies that there should be a mean zero-point shift in the JKT data relative to the INT data of 0.1 mag due to difference in the isophotes used. We therefore apply this shift to all objects observed with the JKT to transform these data to our  $B_{26.1}$  system.

Finally, we investigated the possibility that there could be a small effect due to the change in mean redshift of the samples at fainter magnitudes by searching for a change in the mean galaxy color. Figure 4 shows  $(B_{INT}-R_{INT})$  as a function of  $B_{INT}$ . There is no significant color evolution within the errors: the slope is  $0.005 \pm 0.015$  with a mean  $B - R = 1.62$ .

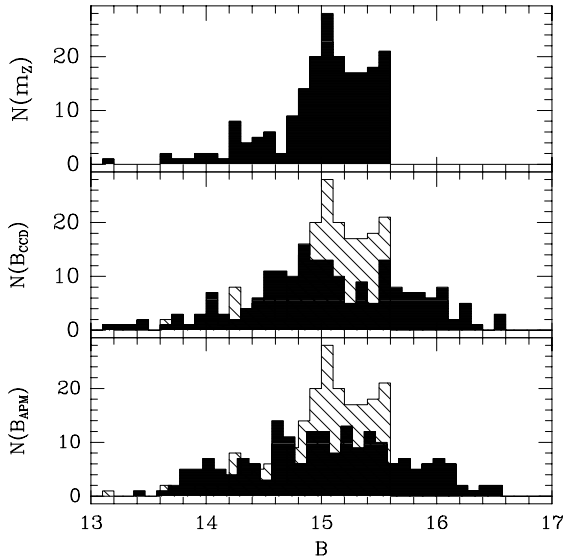


**Figure 5.** Histograms comparing the numbers of galaxies as a function of apparent magnitude  $B$ . Each panel shows in black, from top to bottom, the Zwicky, APM and CCD magnitudes for the same objects. In the lower two panels we also show the Zwicky histogram as a background for comparison.

#### 4 COMPARISON WITH THE ZWICKY CATALOGUE

Bothun & Cornell (1990) have studied the calibration of the Zwicky magnitude scale using a sample of 107 *spiral* galaxies. They suggest that the errors in  $m_Z$  are minimized if  $m_Z$  is an isophotal magnitude at  $B = 26.0 \text{ mag arcsec}^{-2}$ , although it is clear from their Figure 2 that even within such a small sample of objects there is a 5 mag range of isophotes which give isophotal magnitudes corresponding to  $m_Z$ . This suggests that our isophotal detection limit should be optimal for this comparison.

In Figure 5 we show the number counts histograms for the 204 Zwicky galaxies in our sample to the different magnitude systems: Zwicky (top), APM (middle), and CCD (bottom). Comparison of the APM and CCD data shown here suggests that the effect shown in Figure 2 is unlikely to be an artefact of saturation effects in the equatorial APM Survey data at bright magnitudes (see Section 2).

We searched for possible correlations between the magnitude differences,  $B_{CCD} - m_Z$ , and other properties of our sample. The top panel of Figure 6 shows the  $B_{CCD} - m_Z$  difference as a function of CCD color  $B - R$ . The color of Zwicky galaxies is similar to the mean color in Figure 4,  $B - R \simeq 1.6$  and there is no apparent correlation with  $B_{CCD} - m_Z$  within the scatter. This is a useful check, as any large differences that were due to processing errors might be expected to show up as objects of extreme color. The bottom panel of Figure 6 shows the scatter in  $B_{CCD} - m_Z$  as a function of right ascension. Objects were observed in order of increasing RA on each night of our observing run, and so we would expect temporal drifts to show up as a correlation with RA. Again, there is no evidence of any trend. We also investigated possible variations with Galactic latitude (not

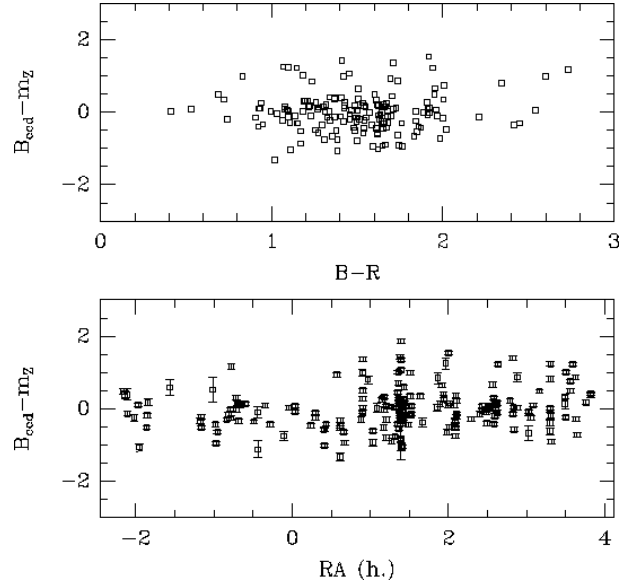


**Figure 6.**  $B_{CCD} - m_Z$  as a function of CCD color  $B - R$  (top panel) and right ascension (bottom).

shown here), and again found no evidence for trends in our data.

Figure 7 is the main result of this paper. It shows the Zwicky magnitude error  $B_{CCD} - m_Z$  as a function of  $B_{CCD}$ , for all Zwicky galaxies with  $B_{CCD} < 17.5$ . For the Zwicky magnitudes we have used a constant error:  $\Delta m_Z = 0.05 \text{ mag}$  (as Zwicky gave his values in units of 0.1 magnitudes). For the CCD we used the error described in Section 3.2. A very similar trend is found for the separate INT and JKT images.

The dashed line in Figure 7 shows a direct least square fit to the data:

$$B_{CCD} - m_Z = 0.6(B_{CCD} - 15.1), \quad (6)$$

which has a scatter of 0.53 mag.

This fit is the result of the interplay between the scatter in the two magnitude systems and the Zwicky survey limit (shown as dotted line in Figure 7). As a result of this scatter, objects with faint  $B_{CCD}$  and bright  $m_Z$  can be included in the survey, but there is a deficit of objects with faint  $m_Z$  and bright  $B_{CCD}$ . i.e. the fit suffers from a Malmquist type of bias. However, for a linear relation, it is apparent that Malmquist bias is insufficient to account for all of the effect shown in Figure 7. We next develop a scheme to correct this fit for the effects of Malmquist bias.

#### 4.1 Malmquist bias correction

Different magnitude system are subject to different systematic errors, and even in the best of the situations intrinsic differences in the morphology, environment and spectrum of the galaxies tend to introduce stochastic fluctuations in any magnitude system. We want to find a best fit linear relation between the Zwicky,  $m_Z$ , and CCD,  $B_{CCD}$ , system:

$$m_Z = \lambda B_{CCD} + Z, \quad (7)$$

where  $\lambda$  will account for any scale difference and  $Z$  is a zero point shift. In general, both  $m_Z$  and  $B_{CCD}$  are stochastic

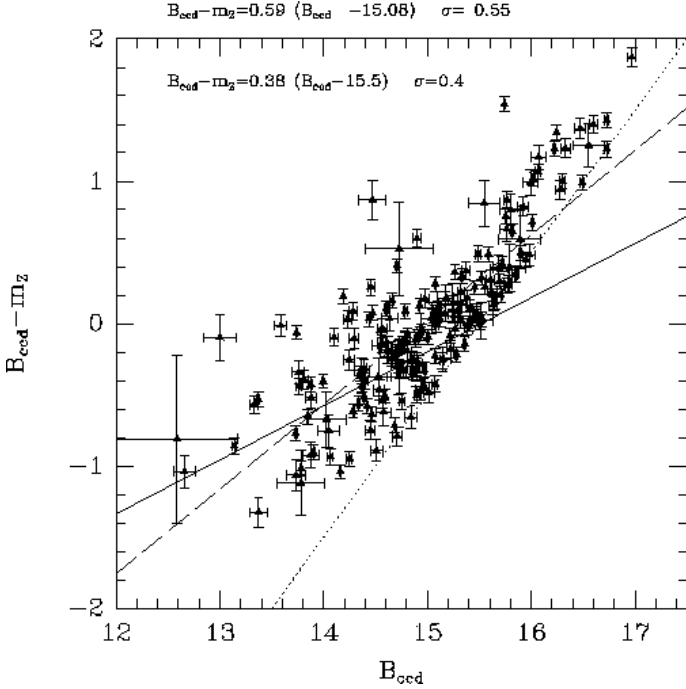


**Figure 7.** The magnitude error  $B_{CCD} - m_Z$  as a function of  $B_{CCD}$ , after correcting Zwicky magnitudes to  $m_Z$ . The dotted line shows the  $m_Z = 15.5$  magnitude limit. The dashed line correspond to a direct least square fit to the data. The continuous line shows the fit corrected for Malmquist bias (see text).

variables and Equation [7] is just a mean relation. As is common practice we will assume that there is Gaussian scatter around the above mean relation (due to the accumulation of multiple uncorrelated factors). That is, given a measured magnitude  $m_Z$ :

$$P(\Delta) = \frac{1}{N} \exp \left[ -\frac{\Delta^2}{2\sigma^2} \right], \quad (8)$$

where  $\Delta \equiv m_Z - \overline{m_Z}$  is a stochastic variate,  $\overline{m_Z}$  is some mean best fit value in the linear relation of Equation [7],  $\sigma$  is the *rms* error and  $N$  is a normalization factor. For a sample that is not magnitude limited we have  $N = \sqrt{2\pi}\sigma$ . For a magnitude limited sample, where  $m_Z < B_{lim}$ , the probability is the same but has a different normalization:

$$N = \int_{-\infty}^{B_{lim} - \overline{m_Z}} dm_Z \exp \left[ -\frac{\Delta^2}{2\sigma^2} \right], \quad (9)$$

because not all magnitudes are possible, so that  $\Delta \equiv m_Z - \overline{m_Z} < B_{lim} - \overline{m_Z}$ . Thus, we can write  $P(m_Z)$  in terms of the complementary error function:

$$P(\Delta) = \frac{2 \exp \left[ -\frac{\Delta^2}{2\sigma^2} \right]}{\sqrt{2\pi} \sigma \operatorname{erfc} \left[ \frac{m_Z - B_{lim}}{\sqrt{2}\sigma} \right]} \quad (10)$$

so that for  $B_{lim} = \infty$  we recover the standard Gaussian result.

We are now able to perform a likelihood analysis to find the best fit values of  $\lambda$  and  $Z$  in the linear relation of Equation [7]. We define a likelihood as:

$$\mathcal{L} = \prod_i P(\Delta_i) \quad (11)$$

where  $i$  runs over all galaxies in the survey, and:

$$\Delta_i = m_Z^i - (\lambda B_{CCD}^i + Z) \quad (12)$$

with  $m_Z^i$  and  $B_{CCD}^i$  the measured Zwicky and CCD magnitudes for galaxy  $i$ . In analogy with the standard  $\chi^2$  test we define a Malmquist bias “corrected chi-square”:

$$\chi_{Malm}^2 \equiv \sum_i \left[ \frac{\Delta_i^2}{2\sigma^2} + 2 \log \left( \operatorname{erfc} \frac{\lambda B_{CCD}^i + Z - B_{lim}}{\sqrt{2}\sigma} \right) \right] \quad (13)$$

Note that the measured magnitude errors,  $\sigma_i$ , are added in quadrature to the stochastic error in the linear relation,  $\sigma$ , which is one of the parameters we want to determine with this fit. The best fit values that we find on maximising the likelihood, using the data in Figure 7, are:

$$\begin{aligned} \lambda &= 0.62 \pm 0.05 \\ Z &= 5.9 \pm 0.7 \\ \sigma &= 0.40 \pm 0.05, \end{aligned} \quad (14)$$

the errors correspond to approximate 99% confidence levels. The values in each uncertainty range are strongly correlated: Lower values of  $\lambda$  (eg larger scale errors) are (linearly) correlated with larger values of  $Z$ , and both are obtained for the smaller  $\sigma$ . The inverse relation gives:

$$B_{CCD} \simeq 1.61 m_Z - 9.5. \quad (15)$$

Figure 7 shows as a continuous line the best fit model for the corresponding best fit magnitude difference:

$$B_{CCD} - m_Z = (0.38 \pm 0.02)(B_{CCD} - 15.53) \pm 0.4 \quad (16)$$

Figure 8 shows the residuals of this fit. For comparison we display a Gaussian with same dispersion,  $\sigma = 0.4$ . As mentioned above the Gaussian does not provide a good fit because the Malmquist bias correction, which produces a deficit of faint objects. It is not possible to show in this Figure a comparison with the Malmquist bias corrected version for the error probability of Equation [10], because this depends not only on the differences,  $\Delta$ , but also on the measured value,  $B_{CCD}^i$ .

Thus, after correcting for the effects of Malmquist bias, the above analysis indicates both a zero-point shift and a change of magnitude scale. The zero point different could be obtained by taking the mean of the magnitude differences over  $m_Z$  magnitudes (which are the ones that define the survey limit):

$$\langle B_{CCD} - m_Z \rangle = -0.35 \pm 0.15. \quad (17)$$

which is in good agreement with Efstathiou *et al.* (1988). The scaling relation between the two magnitude systems is then:

$$\Delta m_Z \simeq (0.62 \pm 0.05) \Delta B_{CCD}. \quad (18)$$

We can also test the above model for the scale error by estimating the magnitude correlations as a function of distance. Figure 9 shows the mean correlation  $\langle \Delta(\theta_i) \Delta(\theta_j) \rangle$  as a function of the pair separation  $|\theta_j - \theta_i|$ , in arcmin. The uppermost panel shows (as continuous lines) the auto-correlation for magnitude differences in the Zwicky system,  $\Delta_i^Z = m_Z^i - \overline{m_Z}$ , where  $m_Z^i$  is the Zwicky magnitude for the

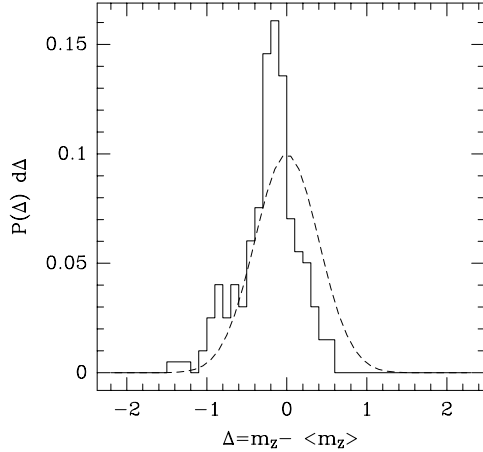


**Figure 8.** The distribution of magnitude errors from the mean linear fit compared to a Gaussian with dispersion  $\sigma = 0.4$ . The Gaussian does not fit the distribution because of the Malmquist bias, which produces a deficit of faint objects.

$i$ th galaxy and  $\overline{m_Z} = \langle m_Z \rangle$  is the mean Zwicky magnitude in the Survey. The middle panel shows the corresponding autocorrelation for the CCD system:  $\Delta_i = B_{CCD}^i - \overline{B}_{CCD}$ . The lower panel shows the autocorrelation of the magnitude errors:  $\epsilon_i = B_{CCD}^i - m_Z^i$ . The long-dashed in each case show the zero values for reference. The short-dashed line in the lower panel shows the prediction based on applying Equation [18] to the data, which is extremely close to the observed result.

We can see in Figure 9 that there is a significant angular correlation between nearby magnitudes and positions with  $\theta \lesssim 5'$ . This correlation is followed by the errors, indicating that the above model is valid. The Zwicky system shows smaller correlations and smaller variance than the CCD system. This can also be understood in the context of the model, as in the Zwicky system the “effective” magnitude scale is about a factor of two smaller (Equation [18]).

Note that at the typical depth of the survey,  $\mathcal{D} \simeq 80 h^{-1}$  Mpc, the above magnitude correlations are only significant at physical scales smaller than  $\lesssim 100 h^{-1}$  Kpc. This correlation has little effect on typical galaxy clustering scales,  $r_0 \simeq 5 h^{-1}$  Mpc, but might be relevant for the inversion of angular clustering on smaller scales. For example, Szapudi & Gaztanaga (1998) find that on scales  $\theta \lesssim 0.1$  degrees there is a significant disagreement between the APM and the EDSGC that is attributed to differences in the construction of the surveys, most likely the dissimilar deblending of crowded fields. At the depth of these Surveys,  $\mathcal{D} \simeq 400 h^{-1}$  Mpc, the above magnitude correlations correspond to  $\theta \lesssim 1'$  and could also have a significant effect on the angular clustering and its interpretation on these small scales.

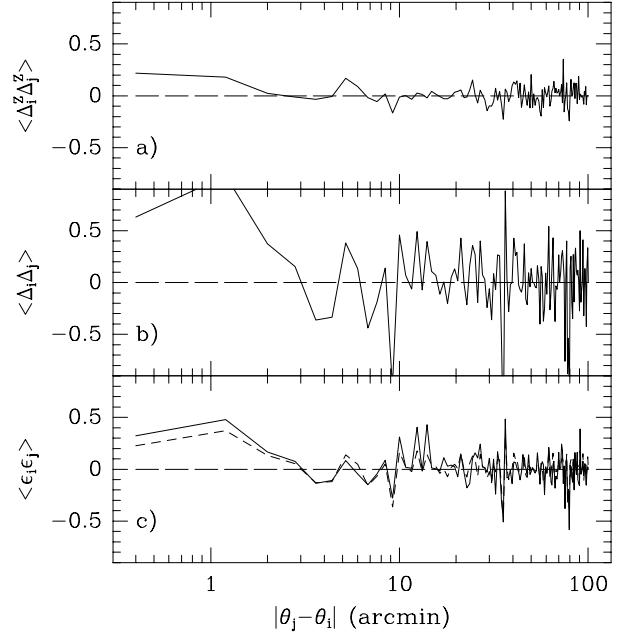


**Figure 9.** Mean correlations in magnitude differences  $\langle \Delta(\theta_i) \Delta(\theta_j) \rangle$  for pairs of galaxies separated by distance  $|\theta_j - \theta_i|$ , in arcmin shown for Zwicky magnitudes (top panel), CCD magnitudes (middle panel), and for the difference  $\epsilon$  between Zwicky and CCD magnitudes (lower panel). The short-dashed line shows the prediction using the scale error model  $\epsilon = 0.6 \Delta B$ . The long-dashed line shows zero correlation for reference.

## 5 PROPERTIES OF NEARBY FIELD GALAXIES

We will now present some further properties of the galaxies in our sample: colors, sizes and ellipticities. This will help us understanding the systematics in the Zwicky magnitude system. As mentioned in the introduction, these local properties are interesting in the context of galaxy evolution and star formation rates. There are still only few samples that are both homogeneous and large enough to provide estimates of the statistical properties of nearby samples (eg see Table 1) most of which have been selected from photographic plates. Our sample is homogeneous enough and extends over a large enough area ( $\simeq 400$  square degrees) to provide a fair sample. Thus the new results based on the CCD magnitudes should be a good local reference for the fainter studies of galaxy evolution.

We will compare the properties of galaxies in the Zwicky ( $m_Z < 15.5$ ) sample with the corresponding properties of galaxies in the INT fields selected using the CCD blue magnitude  $B = B_{CCD}$ . We choose two magnitude cuts:  $B < 16$  which includes most Zwicky galaxies and  $19 < B < 20$ , which includes faint galaxies in the same fields (which are not typically centered around the Zwicky objects).

### 5.1 Sizes and Ellipticities

Figure 10 shows an histogram of the frequency distribution of galaxies as a function of its area (eg number of galaxy pixels in the CCD image). Top panel shows Zwicky selected

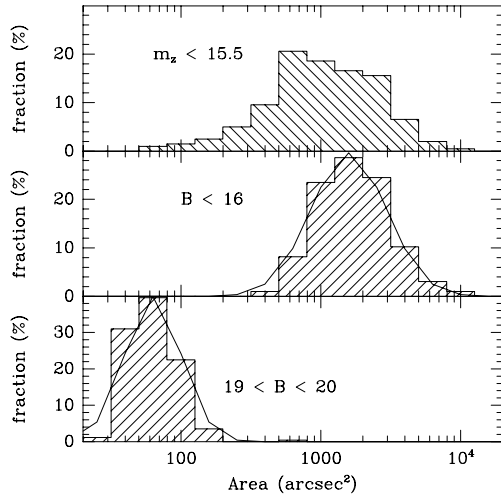


**Figure 10.** Frequency distribution (in per cent) of galaxies as a function of their area (in arcsec<sup>2</sup>) for galaxies selected in different ways: (a) Zwicky sub-sample (top), (b) bright galaxies with CCD magnitudes  $B < 16$  (middle) and (c) faint galaxies with CCD magnitude  $20 < B < 19$  (bottom).

galaxies only. Middle and bottom panels include all the galaxies in the INT fields selected with CCD magnitudes of  $B < 16$  and  $20 < B < 19$ , respectively.

As can be seen in the Figure, Zwicky selected galaxies have a long tail of small objects which is not present in the bright subsample of  $B < 16$  CCD selected objects. This again illustrates the scale error (and selection biases) in the Zwicky system mentioned above (see also the Discussion).

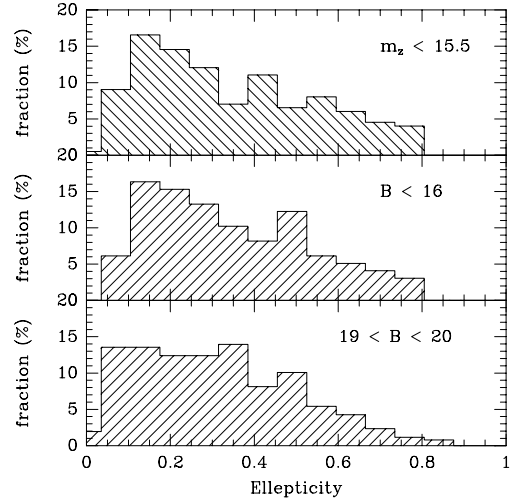
The distribution of sizes in logarithmic scale for both CCD sub-samples are well approximated by a Gaussian (shown as continuous lines in the figure). The mean size is about 60 arcsec<sup>2</sup> for  $20 < B < 19$  and 1600 arcsec<sup>2</sup> for  $B > 16$ , with a rms dispersion of about 20% and 27% respectively.

Figure 11 shows the corresponding frequency distribution for the ellipticities as measure in the galaxy shapes. The frequency distribution of ellipticities in the background galaxies provides crucial information for weak lensing reconstruction. The local distributions seem remarkably similar to the faint one, specially given the large differences in sizes shown in Fig.10. This is a good indication that our isophotes are low enough, as otherwise we would expect a large excess of round faint objects.

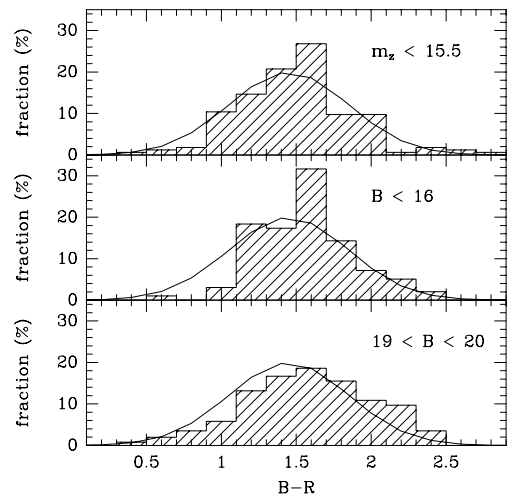
## 5.2 Colors

Figure 12 shows the frequency distribution of CCD color ( $B - R$ ) for the Zwicky galaxies (top panel) in comparison with galaxies in the INT fields selected with CCD magnitudes: with  $B < 16$  (middle panel) and  $20 < B < 19$  (bottom panel). The continuous line in all cases shows for reference a Gaussian distribution with mean  $B - R = 1.45$  and  $\sigma = 0.4$ , which roughly matches the Zwicky frequencies.

The local  $B < 16$  selected distribution seems to be slightly more compact around the peak than the Zwicky set, with a sharper blue edge. This blue edge was also noted by Takamiya et al. (1995).



**Figure 11.** Frequency distribution (in per cent) of galaxies as a function of their ellipticity for galaxies selected in different ways: (a) Zwicky sub-sample (top), (b) bright galaxies with CCD magnitudes  $B < 16$  (middle) and (c) faint galaxies with CCD magnitude  $20 < B < 19$  (bottom).



**Figure 12.** Frequency distribution (in per cent) of galaxies as a function of CCD color  $B - R$  for galaxies selected in different ways: (a) Zwicky sub-sample (top), (b) bright galaxies with CCD magnitudes  $B < 16$  (middle) and (c) faint galaxies with CCD magnitude  $20 < B < 19$  (bottom).

It is also interesting to notice the excess of local galaxies with  $B - R = 1.6$  (specially in the middle panel) and the spread and shift to the red of the faint objects in the bottom panel. These magnitudes are not k-corrected, which could well explain the relative reddening of the faint objects.

## 6 DISCUSSION & CONCLUSION

Marzke et al. (1994) used a Monte Carlo method to estimate how the LF parameters would change if the dispersion  $\sigma_M$  were 0.65 mag (closer to what we find than the nominal



0.3 mag they used). They conclude that the *true*  $M_*$  should be about 0.6 mag brighter, and that a similar conclusion would be reached for a small scale error. Marzke et al. use this estimate to conclude that a combination of incompleteness and a small (0.2 mag) scale error would be sufficient to move the CfA2-North values to those found from CfA2-South. Takamiya et al. (1995) find evidence for a large scale shift between Volume I and Volumes II and V of the Zwicky catalogue. This shift appears to be of order 0.5 mag mag<sup>-1</sup> over the range  $14 < m_Z < 15.7$ , which is comparable to our findings for Volume V, although they find very little effect for Volumes II and V. However, we note that Figure 4 of Takamiya et al. shows  $B - m_Z$  vs.  $B$ , rather than  $m_Z$ . A similar representation of Figure 7 of this paper looks very similar to Figure 4a of Takamiya et al., which is reasonable, given that Figure 7 implies a strong compression of the  $m_Z$  axis, which effectively hides the scale error. Unfortunately, the overlap between the 204 objects in our sample and the 155 objects in the Takamiya et al. data is too small to draw any detailed comparison, given that there are  $\sim 600$  Zwicky galaxies within the region of our survey.

In this paper we have presented CCD magnitudes for galaxies around 204 Zwicky galaxies. We find evidence for a significant scale error as pointed out by Bothun & Schommer (1982) and Giovannelli & Haynes (1984). This is found by direct likelihood analysis, corrected for Malmquist bias, and also by noticing the angular correlations between the errors (Fig.9) or the long tail of small objects in the frequency distributions of sizes (Fig.10). The mean scale magnitude error is quite large:  $\Delta m_Z \simeq 0.62 \Delta B_{CCD}$ , while the mean zero point is about  $-0.35$  (Equation [17]), in agreement with Efstathiou *et al.* (1988).

A detailed analysis of the implications of these calibrations on the LF would require the redshift information and is left for future work. Nevertheless it is possible to use the mean relation to show how we expect the LF to change. The scale error will reduce the amplitude of the LF by a factor  $\lambda \simeq 0.62 \pm 0.05$ . For the CfA2 South results of Marzke et al. (1994) this gives:

$$\phi_*(corrected) = \lambda \phi_* \simeq 0.0124 \pm 0.006 h^3 \text{ Mpc}^{-3} \quad (19)$$

while the zero point will change  $M_*$ :

$$M_*(corrected) = M_* + Z \simeq 19.3 \pm 0.3. \quad (20)$$

If applied to the LF for the whole CfA2 survey, these numbers would imply:

$$\phi_*(corrected) = \lambda \phi_* \simeq 0.025 \pm 0.009 h^3 \text{ Mpc}^{-3} \quad (21)$$

$$M_*(corrected) = M_* + Z \simeq 19.10 \pm 0.21, \quad (22)$$

where we have added the errors in quadrature. Thus the corrected values are now closer the SAPM and LCRS. This can be seen in Figure 13 which should be compared with the uncorrected version of Figure 1.

An illustration of the scale error in the Zwicky system can be seen in the galaxies shown in Figures 15 and 14. Table 3 gives the Zwicky and CCD magnitudes for each of the Zwicky galaxies as labelled in the Figures. As can be seen from the table, the range of Zwicky galaxies in Figure 14 is  $\Delta m_Z = 0.3$  which is almost 6 times smaller than the CCD range  $\Delta B_{CCD} = 1.7$ . The range for the whole cluster is  $\Delta m_Z = 1.3$ , almost a factor of 3 smaller than the

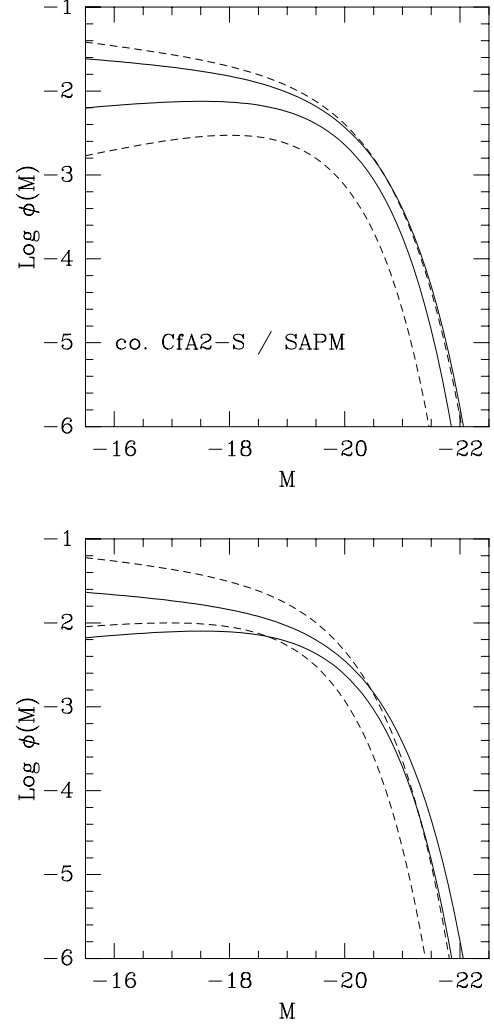


**Figure 13.** Luminosity function estimations. The continuous lines enclose the 2-sigma region in the SAPM estimation whereas the dashed lines enclose the 2-sigma region in the CfA2 estimation after correction for the model of the Zwicky magnitude system and errors. The upper panel shows the corrected LF for CfA2-South, and the lower for the whole CfA2 survey.

CCD range:  $\Delta B_{CCD} = 3.5$ . These illustrations are strongly suggestive of an observer-bias effect, whereby some fainter galaxies are included in the same due to their proximity to brighter objects, e.g. object #9 in Figure 15. This bias can also be seen in statistical terms as a long tail of small objects in the frequency distribution of Fig.10.

### Acknowledgements

The Isaac Newton Telescope (INT) and Jacobus Kapteyn Telescope (JKT) are operated on the island of La Palma by the Isaac Newton Group in the Spanish Observatorio del Roque de los Muchachos of the Instituto de Astrofísica de Canarias. We thank Steve Maddox, Will Sutherland, John Loveday, Cedric Lacey, Michael Vogeley, Dick Fong, and Nigel Metcalfe for useful discussions. This work has been supported in part by CSIC, DGICYT (Spain), projects PB93-0035 and PB96-0925, and by a bilateral collaboration (Accion Integrada HB1996-0091) between CSIC

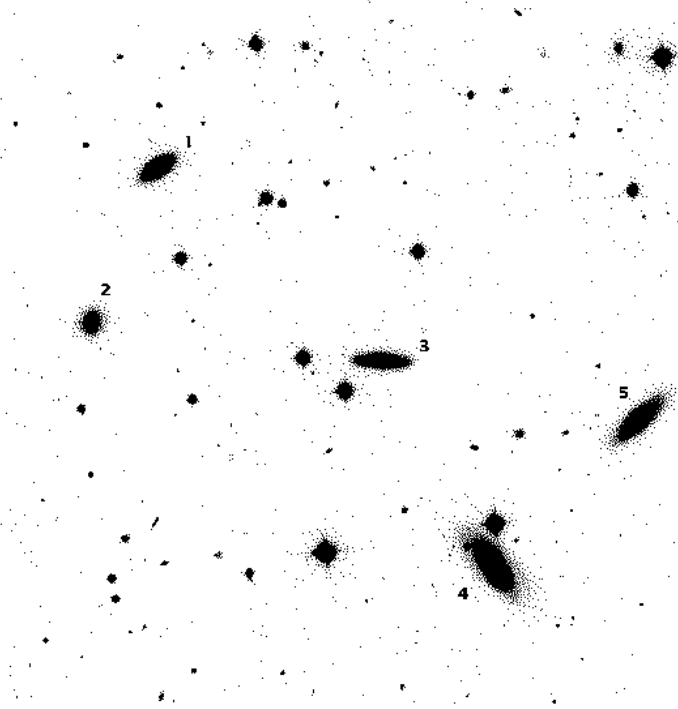


**Figure 14.** A CCD image (in *B*) containing several Zwicky galaxies (labeled with numbers) in a rich cluster.

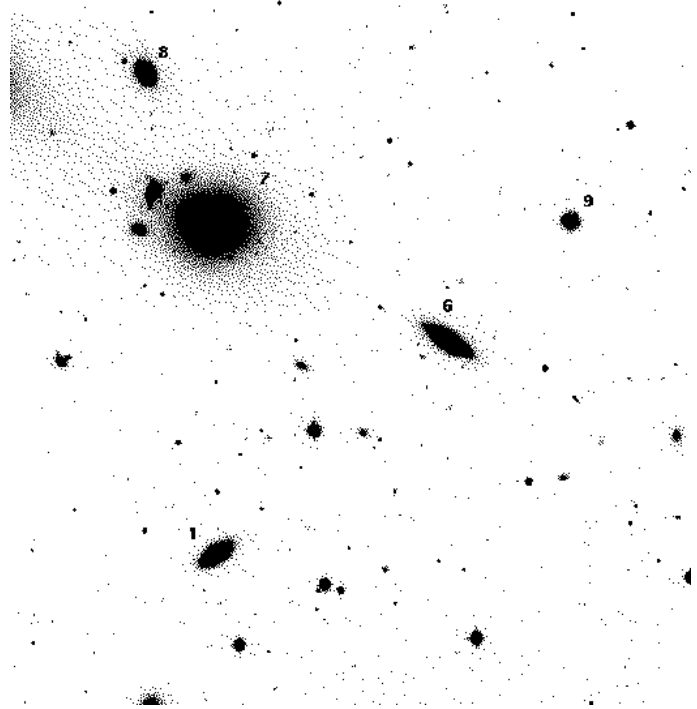


**Figure 15.** A CCD image (in *B*) containing several Zwicky galaxies (labeled with numbers) in a rich cluster.

Galaxy #	Zwicky $m_Z$	CCD <i>B</i>
1	15.0	15.0
2	15.0	16.1
3	14.8	15.1
4	14.7	14.4
5	14.8	14.9
6	14.9	14.8
7	14.0	13.2
8	15.2	14.9
9	15.3	16.7

**Table 3.** Comparison of CCD and Zwicky magnitude for galaxies, as labeled in Figures 14 and 15.

(Spain) and the Royal Society (UK). Part of the data reduction and analysis was carried out at the University of Oxford, using facilities provided by the UK Starlink project, funded by the PPARC.

## 7 REFERENCES

- Blair, M., & Gilmore, G., 1982, *PASP*, 94, 7423  
 Bothun, G.D., & Cornell, M.E., 1990, *AJ*, 99, 1004  
 Bothun, G.D., & Schommer, R., 1982, *ApJ*, 255, L23  
 Da Costa, L.N., Geller, M.J., Pellegrini, P.S., Latham, D.W., Fairall, A.P., Marzke, R.O., Willmer, C.N.A., Huchra, J.P., Calderon, J.H., Ramella, M., Kurtz, M.J., 1994, *ApJ*, 424, L1  
 Efstathiou, G., Ellis, R.S., & Peterson, B.J., 1988, *MNRAS*, **232**, 431  
 Folkes, S., Ronen, S., Price, I., Lahav, O., Colless, M.M., Maddox, S.J., Deeley, K., Glazebrook, K., Bland-Hawthorn, J., Cannon, R.D., Cole, S.M., Collins, C.A., Couch, W.J., Driver, S.P., Dalton, G.B., Efstathiou, G., Ellis, R.S., Frenk, C.S., Kaiser, N., Lewis, I.J., Lumsden, S.L., Peacock, J.A., Peterson, B.A., Sutherland, W.J., Taylor, K., 1999, *MNRAS*, in press  
 Geller, M.J., Kurtz, M.J., Wegner, G., Thorstensen, J.R., Fabricant, D.G., Marzke, R.O., Huchra, J.P., Schild, R.E., Falco, E.E., 1997, *AJ*, 114, 2205  
 Giovanelli, R., & Haynes, M.P., 1984, *AJ*, 89, 1  
 Hamuy, M., & Maza, J., 1989, *AJ*, 97, 720  
 Huchra, J.P., Davis, M., Latham, D. & Tonry, J. 1983, *ApJS*, 52, 89  
 Landolt, A.U., 1992, *AJ*, 104, 340  
 Lin, H., Kirshner, R.P., Sheckman, S.A., Landy, S.D., Oemler, A., Tucker, D.L., Schechter, P.L., *ApJ*, **464**, 60  
 Loveday, J., Peterson, B.A., Efstathiou, G., & Maddox, S.J., 1992, *ApJ*, **390**, 338  
 Maddox, S.J., Sutherland, W.J., Efstathiou, G., & Loveday, J., 1990, *MNRAS*, **242**, 43P  
 Maddox, S.J., Sutherland, W.J., Efstathiou, G., & Loveday, J., 1991, in *“The Early Observable Universe from Diffuse Backgrounds”*, eds. Rocca-Volmerange, B., Deharveng, J.M., & Trần Thanh Vân, J.  
 Maddox, S.J., Sutherland, W.J., Efstathiou, G., & Loveday, J., 1990a, *MNRAS*, **243**, 692  
 Maddox, S.J., Sutherland, W.J., Efstathiou, G., & Loveday, J., 1990b, *MNRAS*, **246**, 433

- Maddox, S.J., Sutherland, W.J., Efstathiou, G., Loveday, J.,  
& Peterson, B.A., 1990, *MNRAS*, **247**, 1P
- Marzke, R.O., Huchra, J.P., & Geller, M.J., 1994, *ApJ*, **428**,  
43
- Metcalfe, N., Fong, R., & Shanks, T., 1995, *MNRAS*, 274,  
769
- Peterson, B.A., Ellis, R.S., Efstathiou, G., Shanks, T., Bean,  
A.J., Fong, R., & Zen-Long, Z., 1986, *MNRAS*, 221, 233
- Schechter, P., 1976, *ApJ*, **203**, 297
- Szapudi, I., Gaztanaga, E., 1998, *MNRAS* 300, 493
- Takamiya, M., Kron, R.G., & Kron, G.E., 1995, *AJ*, 110,  
1083
- Zucca, E., Zamorani, G., Vettolani, G., Cappi, A., Merighi,  
R., Mignoli, M., Stirpe, G.M., MacGillivray, H.,  
Collins, C., Balkowski, C., Cayatte, V., Maurogordato,  
S., Proust, D., Chincarini, G., Guzzo, L., Maccagni,  
D., Scaramella, R., Blanchard, A., Ramella, M., 1997,  
*A&A*, 326, 477
- Zwicky, F., Herzog, E., Wild, P., Karpowicz, M., & Kowal,  
C.T., 1968, *Catalogue of Galaxies and Clusters of  
Galaxies*.